Journal of Applied Physics

Research on efficient and stable control of EUV-induced hydrogen plasma

Cite as: J. Appl. Phys. **131**, 233301 (2022); https://doi.org/10.1063/5.0088669
Submitted: 19 February 2022 • Accepted: 22 May 2022 • Published Online: 16 June 2022

Qijun Mao, Xuepeng Gong, Qipeng Lu, et al.

Journal of Applied Physics ARTICLE scitation.org/journal/jap

Research on efficient and stable control of EUV-induced hydrogen plasma

Cite as: J. Appl. Phys. **131**, 233301 (2022); doi: 10.1063/5.0088669
Submitted: 19 February 2022 · Accepted: 22 May 2022 ·
Published Online: 16 June 2022

View Online Export Citation CrossMark

Qijun Mao,[1,2] Xuepeng Gong,[1,a)] Qipeng Lu,[1,a)] Yuan Song,[1] Dazhuang Wang,[1] Yang Bai,[1,2] and Tianyu Ma[1,2]

AFFILIATIONS

[1]State Key Laboratory of Applied Optics, Changchun Institute of Optics, Fine Mechanics and Physics, Chinese Academy of Sciences, Changchun 130033, China
[2]University of Chinese Academy of Sciences, Beijing 100049, China

[a)]**Authors to whom correspondence should be addressed:** gongxuepeng120@foxmail.com and luqipeng@126.com

ABSTRACT

We use the numerical model to study the control method for the ion sputter flux and energy at the surface of multilayer mirrors in hydrogen plasmas induced by extreme ultraviolet (EUV) radiation. This plasma is generated via photoionization by EUV photons with wavelengths at 13.5 nm and collision ionization by high-energy electrons. An electric field is formed by applying different bias voltages to the cylindrically symmetrical cavity and sample holder, which guides the transfer of charged particles and increases their energy. The evolution of pulsed EUV-induced plasma under the field is described by a two-dimension particle-in-cell model and the Monte Carlo simulation to represent collisions between charged particles and background molecules. The results show that the distribution of the electric field varies during the pulse and point out that the secondary electrons, which gain energy from the varying field and generate more plasma by collisions with hydrogen molecules, are crucial plasma sources in this scheme. We then propose a stable and efficient control method for EUV-induced hydrogen plasma by optimizing the cavity structure as an ellipsoid and treating the surface of the cavity in contact with the plasma.

I. INTRODUCTION

Reflective optics are often polluted by carbon depositions adsorbed on the surface, which seriously affects their service life and reflectivity in extreme ultraviolet lithography (EUVL) tools.[1] This phenomenon also occurs in synchrotrons operating in the EUV spectrum range.[2] Although a high-vacuum environment is required in EUVL tools, hydrocarbons (C_xH_y) are still present at about 10^{-8} Torr due to the volatility of organics such as photoresists.[3] These hydrocarbons are cracked by absorbing high-energy (92 eV) photons, leaving carbon atoms attached to the surface of multilayer mirrors (MLMs).[4] The growth rate of carbon deposition can reach 0.001–0.01 nm/h.[5] The theoretical limit of reflectivity from EUV MLMs is 74% and, in practice, is about 70%.[6] A 2-nm-thick carbon deposition causes about a 1% drop in reflectivity, and for an optical system with four mirrors for illumination and six mirrors for reflection, the overall reflectivity will drop by 15%. The current methods to clean carbon deposition (radio frequency plasma sputtering and atomic hydrogen cleaning) all require interruption of the working process and changing the working environment of the EUV lithography machine. EUV-induced plasma has been proposed for *in situ*, non-destructive, and efficient carbon cleaning from MLM surfaces in recent years.

Microwave cavity resonance spectroscopy, a non-intrusive detection method that can accurately monitor the spatiotemporal distribution of electron density in plasma, is used to study EUV-induced plasma.[7,8] The effectiveness of EUV-induced plasma in removing the carbon attached to MLM surfaces was validated for the PROTO-2 platform,[9,10] which has significant implications for the practical application of this particular type of plasma. The evolution of EUV-induced plasma in a microwave cavity and PROTO-2 was also studied numerically by the particle-in-cell with Monte Carlo collisions (PIC-MCC) simulation.[11,12] The photoelectrons and secondary electrons (SEs) must be considered to improve the accuracy of the simulations.

This paper proposes a management scheme for carbon cleaning on optical surfaces in EUVL tools by EUV-induced hydrogen plasma. The cleaning scheme and numerical tools are presented in Secs. II and III, respectively. The results of numerical simulations of ion sputtering of the MLM surface are discussed in Sec. IV as a function of the structure of the grounded cavity, the material of the

inner surface of the cavity, and the bias voltage applied to the sample holder. We thus obtain a method for managing the ion flux and energy on the MLM surface, which lays the foundation for further applications for *in situ* and online carbon cleaning for the EUV optics.

II. ESTABLISH THE CONTROL SCHEME

In EUVL tools, about 30% of the EUV intensity is lost at each reflection.[6] In hydrogen gas below 100 Pa, the EUV photon absorption rate is essentially proportional to the gas pressure according to the Beer–Lambert law. To maintain the intensity of the EUV beam during propagation, the working pressure of hydrogen gas should be as low as possible, and no interfaces should be introduced into the beam path.

Figure 1 shows the scheme for applying the electric field. The metal cavity is grounded, so the potential is zero. When a negative bias voltage is applied to the sample holder, an electric field is formed between the grounded cavity and the sample holder. The ions transport to and sputter the surface of the MLM sample under the influence of the electric field. In Fig. 1, the grounded cavity on the left is a cylindrical structure with a diameter of 40 mm and a height of 50 mm. The ellipsoidal one on the right reduces the diameter of the top aperture to 16 mm. The MLM sample is fixed to the holder by a quartz ring with an inner diameter of 16 mm, and the insulating sleeve protects the holder from plasma erosion. A 13.5 nm EUV beam irradiates the sample surface from the normal direction, and the hydrogen molecules in the beam path will be photoionized.

Table I summarizes the basic parameters of the EUV source, which is xenon-discharge pulsed. The temporal pulse width is 1 ms, and the EUV irradiation lasts only 100 ns. Therefore, the EUV-induced plasma will undergo a complex evolution during each pulse before disappearing.

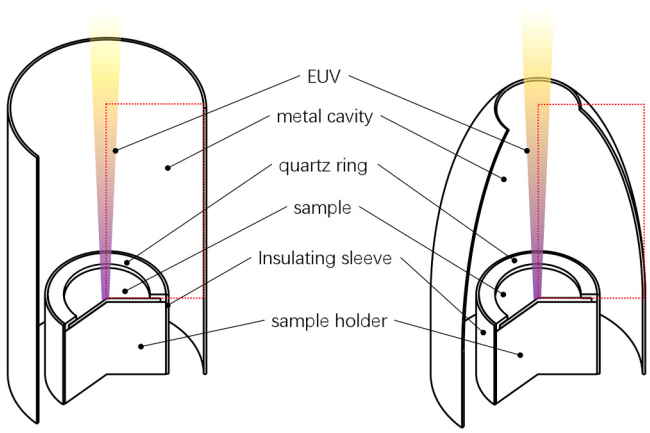

FIG. 1. Configuration of simulation area, cylinder grounded cavity on the left, and ellipsoid on the right. The sample is fixed with a quartz ring onto the sample holder, and an insulating sleeve protects the sample holder from plasma attack.

TABLE I. Basic parameters of EUV source.

Parameter	Value
Wavelength	13.5 nm
Focus diameter	4 mm
Pulse energy	10 μJ/mm^2
Pulse frequency	≈1 kHz
Pulse duration	100 ns

III. COMPUTATIONAL MODEL

The direct photoionization by EUV photons (the background of these schemes is hydrogen) is a prerequisite for forming EUV-induced plasma. This phenomenon has not been detected in lithography tools operating at wavelengths of 193 nm or longer. The photoelectrons emitted from the irradiated area of MLM and the SEs emitted from solids will affect such plasma. The EUV-induced phenomena in the schemes, which are coaxial in Fig. 1, are simulated in the area represented by the red dashed box by the two-dimensional PIC-MCC in cylindrical coordinate. Our PIC model follows the general scheme in Ref. 13, which is compared with the experiment and verified below. The empirical formula of the ion-induced physical sputtering yields from solids at normal incidence is presented.[14] Nevertheless, it is difficult to determine the appropriate fitting parameters for the complex physical and chemical interaction between hydrogen ions and carbon atoms. Chemical sputtering will dominate when the hydrogen ion energy is low.

A. Direct EUV photoionization

When a 13.5 nm EUV beam irradiates low-pressure hydrogen gas, the gas molecules are ionized by photons of 92 eV energy and produce energetic (~75 eV) electrons and heavy masses (H^+, H_2^+), accompanied by plasma glow.[15] Proportionality is obtained according to the calculation of each photoionization reaction cross section,[16–18]

$$hv{:}e{:}\ H^+{:}\ H_2^+ \approx 1{:}1.05{:}0.25{:}0.8, \tag{1}$$

where hv represents photons that collide with hydrogen molecules. The production of each species in the plasma can be obtained by calculating the number of photons absorbed (depending on the photoionization cross section). The density of electrons generated by photoionization n_e is

$$n_e = \frac{N_{pe} n_{gas} \sigma_{pi} I_0 (1 + R)}{E_{ph}}, \tag{2}$$

where N_{pe} is the average number of high-energy electrons excited by each absorbed EUV photon, which is 1.05 according to Eq. (1). n_{gas} is the background gas molecular density, and I_0/E_{ph} is the photon flux. After reflection from the MLM (the reflectivity R is about 0.7), the total production is multiplied by (1 + R).

B. Particle collisions

During the propagation of plasma, various collisions between particles lead to the attenuation of particle energy, the disappearance, and the generation of matters. This work considers six major collisions between high-energy electrons and hydrogen molecules, as shown in Fig. 2, where the data for the cross sections are taken from Refs. 19 and 20. These processes are accurately simulated by the Monte Carlo collisions.

The collisions between heavy masses and neutral H_2 are dominated by elastic collisions. The proton hop collision converted H_2^+ to H_3^+ within 0.5 μs, resulting in H_3^+ becoming the most dominant ion in EUV-induced hydrogen plasma.[21]

C. The external photoelectric effect induced by EUV

The reflective optics of EUVL tools are covered with 2 nm of ruthenium (Ru) as an antioxidant cap.[22] Due to the external photoelectric effect of Ru, the cap readily ejects photoelectrons upon irradiation by EUV.[23] The energy distribution of photoelectrons is independent of the photon energy but is related to the work function of the material. When the work function is 5 eV, the energy distribution is shown in Fig. 3, where most of the photoelectrons have energies of only a few eV.[24]

As shown in Table II, the photoelectron yield (average number of photoelectrons produced per incident photon) of different surface states, such as clean ruthenium, ruthenium exposed to air, oxidized ruthenium, and ruthenium covered with a carbon layer, of the Ru cap upon irradiation at 13.5 nm are detected.[4] After the carbon is deposited on the cap, the photoelectron yield decreases slightly.

In our model, the value of the photoelectron yield is set at 0.013. The applied electric field is directed from the inner wall of the cavity to the sample surface, which propels the photoelectrons to transport to the inner wall of the cavity. The photoelectrons gain energy from the field and ionize more hydrogen plasma during the transport.

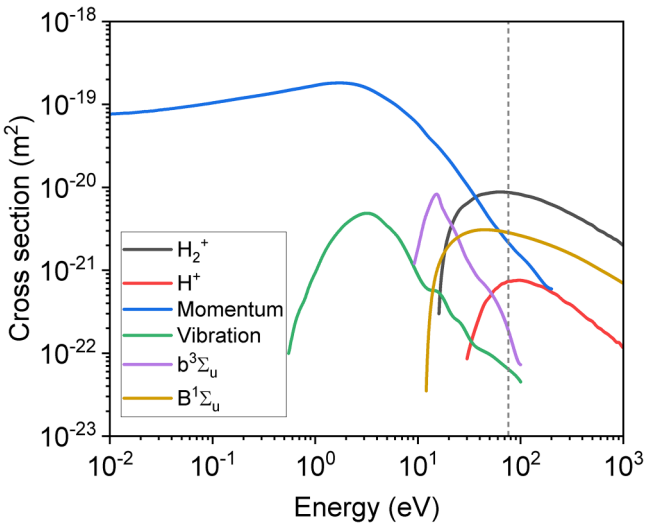

FIG. 2. Cross sections as a function of electron energy for collisions between electrons and hydrogen molecules.

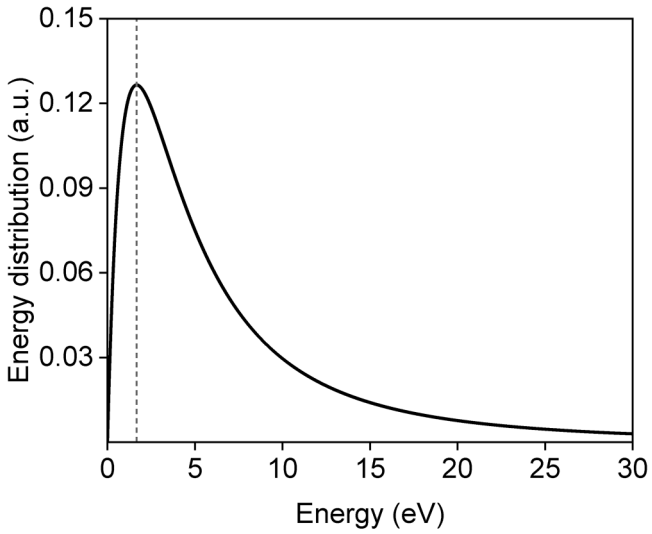

FIG. 3. Energy distribution of SEs emitted from solids.

D. Secondary electron emission

Secondary electron emission (SEE) induced by electron impact on the surface of solids, especially cavity, is considered. The mechanism of SEE caused by electrons is similar to that of photoelectron emission caused by photons. In SEE, the incident electrons not only excite free electrons but also elastically collide in the solid. Some of them returned to free space, which is the background scattering of the incident electrons. The escape of excited free electrons and the background scattering of incident electrons co-occur and are indistinguishable.[25]

The secondary electron yield (SEY), representing the average number of SEs induced per primary electron (i.e., incident particle), has a specific functional relationship with the primary electron energy E_{pe}. The E_{pe} value corresponds to the maximum yield δ_m of the material is denoted E_m. The SEY of materials is affected by different surface states. For example, δ_m of a generally clean metal surface is less than three, but when the surface is oxidized or otherwise treated, δ_m increases by several orders of magnitude.[26] The incident angle of the primary electron also affects the SEY, which was described detailed in Ref. 27.

TABLE II. Photoelectron yield of different surface conditions of Ru cap.[4]

Ru condition	Photoelectron yield
Clean Ru	0.021 ± 0.02
Air-exposed Ru	0.030 ± 0.04
O-covered Ru	0.025 ± 0.04
C-covered Ru	0.017 ± 0.04

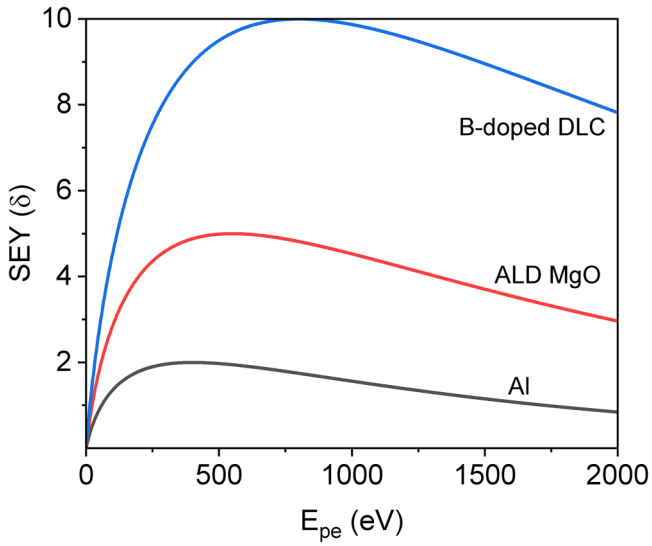

FIG. 4. SEY of clean Al, ALD MgO, and B-doped diamond-like carbon.

Figure 4 plots the SEY vs E_{pe} for clean metal aluminum[28] and the same with two surface treatment materials, atomic layer deposition (ALD) MgO and B-doped diamond-like carbon.[26,27] Both materials exhibit high SEY and stable secondary electron emission and are applied as the surface coatings to photomultiplier dynodes. The introduction of high-SEY materials is beneficial for studying how SEs affect the evolution of EUV-induced plasma.

Most ions bombard the sample with an energy of about 200 eV since a bias of −200 V is applied to the sample holder. The energy of ions diffusion to the cavity surface is usually tens of eV, which depends mainly on the potential of the optical path region. The electron emission from metals induced by ions is not negligible in the model, despite relatively small yields for this energy range.[29] According to Ref. 30, we set the electron emission yield induced by ions from the sample to 0.1 and the cavity to 0.05. Plasma decay processes such as surface absorption, energy decay, and others[31] are also considered in our model.

E. Validate the model

The efficiency of carbon cleaning by EUV-induced hydrogen plasma in PROTO-2 has been measured.[32] Our model is flexible and can adapt to simulate the evolution of EUV-induced plasma in PROTO-2 by only modifying the chamber structure and the EUV source spectrum in our model. By comparing the measured results, the correctness of the model is verified.

The ion flux on the sample surface is counted under the bias voltage of −50, −100, and −200 V at 3 Pa hydrogen. The average sputtering rates (C atom per hydrogen ion) are 0.5, 0.6, and 1.9, accordingly.[32] The maximum etched depth and total etched volume of 10^7 pulses are obtained. The density of amorphous carbon produced on the surface of MLM under EUV irradiation is about 1.9 g/cm^3, which is related to the etched depth.[9]

Table III compares the carbon removal rate between experiments and simulations. It is reported that the simulation error is less than 20% at −100 and −200 V, and the deviation is relatively large at −50 V. According to the mechanism, the realistic electron emissivity should be lower than that of the model (Sec. III D) as the energy obtained by ions decreases. This model correctly counts the carbon removal rate on the exposed surface in PROTO-2, reflecting the reliability of simulating plasma evolution.

Therefore, a series of simulations were carried out under different conditions to understand the evolutions of the EUV-induced plasma in our management scheme.

IV. RESULTS AND DISCUSSION

A. Evolution of induced plasma during a single pulse

We now discuss the simulation of the plasma evolution during a single EUV pulse inside the grounded cylindrical cavity structure with 3 Pa hydrogen pressure. The sample holder is biased at −200 V, and the cavity is made of aluminum with an untreated surface. Figure 5 shows the calculated results for the potential and the electron density in the first 0.5 μs. The potential distribution at 0.5 ns is considered for charge neutrality. During the first 100 ns EUV irradiation, plasma is continuously induced in the optical path, and photoelectrons are continuously emitted from the irradiated area of the sample. The electrons rapidly fill the interior space of the cavity under the combined motion of density diffusion and field drift. The ions move slowly because of their large mass and low energy. The difference in mobility between the two opposite charges leads to an increase in the positive-charge density in the beam path, so the potential rises by several tens of eV, which dumps the outward movement of electrons and accelerates that of ions. The potential is slightly lower than −200 V because of the sizeable negative charge density formed by photoelectrons adjacent to the sample. After irradiation, no more electrons are induced by EUV photons, and the potential rises rapidly in a short time (about 100 ns) due to the escape of electrons. With the collisions and

TABLE III. Comparison of carbon removal rate with experimental results.

	Max etched depth nm/10^7 pulse		Etched volume 10^{-6} cm^3/10^7 pulse	
Bias (V)	Measured[32]	Simulation	Measured[32]	Simulation
−50	∼1.7	2.14	∼0.03	0.047
−100	∼5.7	4.74	∼0.1	0.096
−200	∼14	16.7	∼0.3	0.31

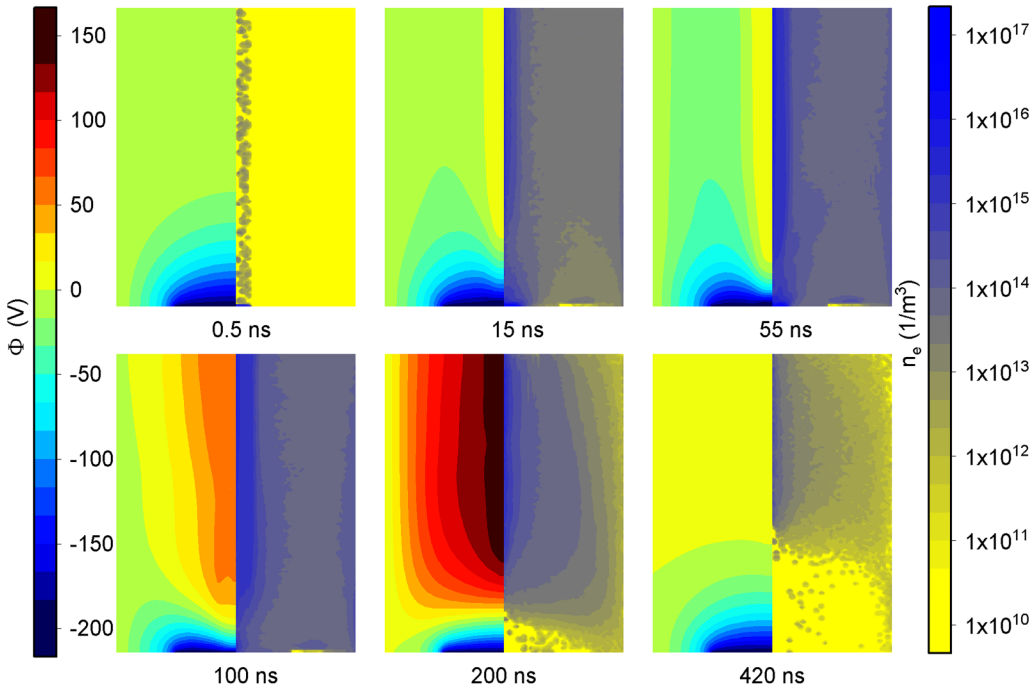

FIG. 5. Evolution of electric field (left side of each panel) and transformation of electron density distribution (right side of each panel) during the first half microsecond in a cylindrical cavity with 3 Pa hydrogen pressure and a sample holder bias voltage of −200 V.

other surface reactions of the plasma, charge neutrality is restored, the electric field returns to the initial state, and the electron density distribution gradually becomes a function of the field.

We also simulated different hydrogen pressure conditions. Figure 6 shows the fluxes of H_3^+ sputtering at the sample surface within 1 μs. As the three solid lines, the ion fluxes increase rapidly during the irradiation period (the first 100 ns) and begin to decay as the irradiation ends. When the pressure is 3 Pa, the flux of the solid red line rises to another peak about 200 ns after the irradiation, compared to the case where no SEs are generated from the cavity surface represented by the orange dotted line. It is found that while the field varies, the SEs transport toward the central axis of the cavity, gaining energy and ionizing more plasma, thus increasing the sputtering ion flux on the sample surface.

From the latter case (the orange dotted line), it can be seen that in addition to the SEs generated from the cavity surface, other electron emission processes are also critical. The SEs emitted from other solid surfaces and electron emission induced by ions would also ionize the molecules, maintaining the ion flux during 200–300 ns.

These simulation results indicate that the SEs generated from the aluminum cavity surface significantly improve the total yield of EUV-induced plasma. Methods for enhancing the yield of SE on the cavity surface should be followed to improve the yield of plasma and the ion flux on the sample surface. Therefore, we changed the cavity structure, treated the aluminum surface, and carried out a series of simulations. The effects of these modifications to the scheme on EUV-induced plasma are discussed in detail below.

B. Influence of cavity structure

During charge transport, the sharp variation of space potential in the cavity cannot be effectively suppressed due to the diameter of the top aperture being too wide when the cavity structure is cylindrical. Optimizing the structure of the cavity from a cylinder to an ellipsoid, as shown on the right side of Fig. 1, effectively limits the rise of the potential.

Figure 7 shows the results of a simulation of the distribution evolution of the potential and electron density induced by EUV photons in the ellipsoid cavity over the first 0.5 μs under the same conditions in Sec. IV A. As shown in Fig. 5, in the cylindrical cavity, the potential rapidly rises to about 150 V after EUV irradiation, accelerating the transport of positive ions to the cavity and decreasing the efficiency of ions sputtering the sample surface. The ellipsoid structure increases the field strength perpendicular to the surface of the sample. The decrease of the inner diameter of the aperture strongly limits the rise of the potential (50 V at highest) inside the cavity. Therefore, the transport of ions to the cavity is much slower than that of the cylindrical structure. These cause a change in the electric field, which drives more positive ions to sputter to the surface of the sample.

The different distributions of the electric field between the two cavities also affect the energy of ions sputtering on the sample

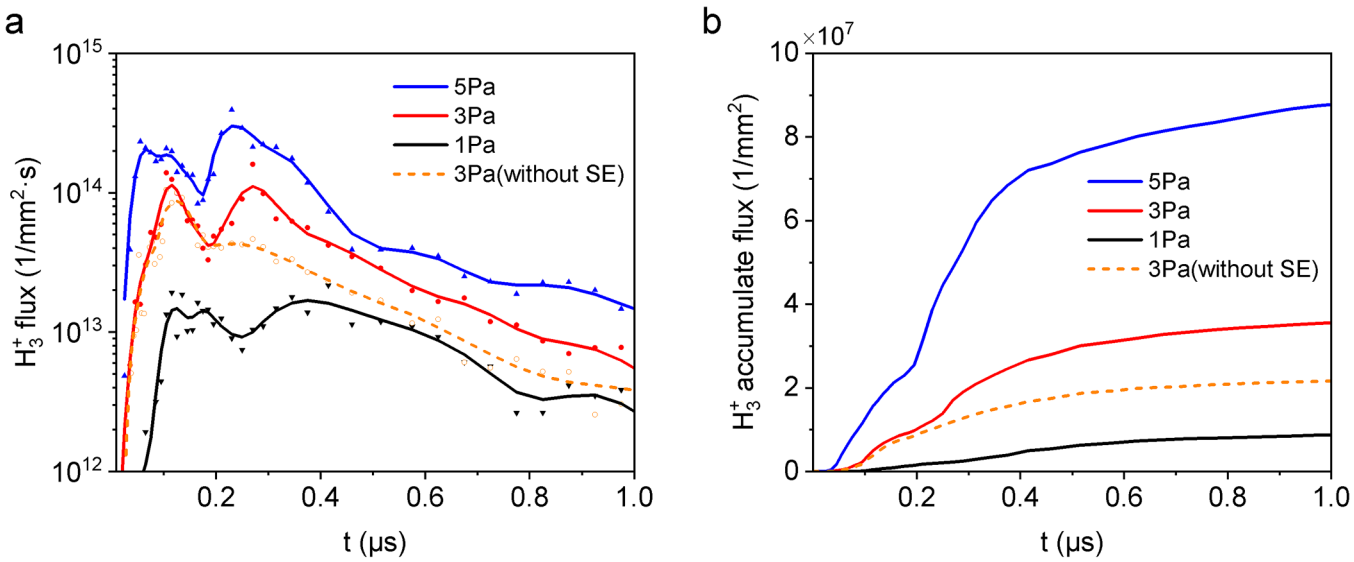

FIG. 6. (a) Simulated H_3^+ fluxes at the sample surface under different hydrogen pressure, and (b) accumulated H_3^+ fluxes.

surface. In each PIC step, our model not only simulates the changes in particle position and velocity but also updates the energy changes of particles (gained from the electric field). This model allows particle flux and energy to be recorded at any position in the simulation area, including the sample surface. Thus, the average energy of the ion attack sample can also be obtained. Figure 8 shows the average energy of H_3^+ attacking the sample surface along the radial direction in the two structures where the

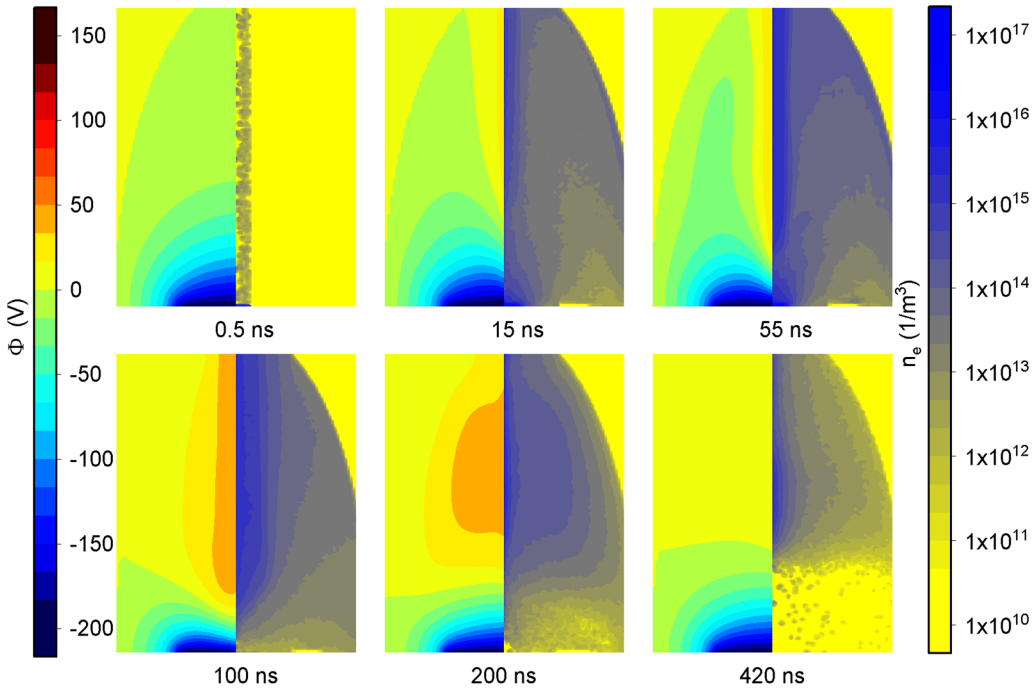

FIG. 7. Evolution of electric field and transformation of electron density distribution during the first half microsecond in an ellipsoidal cavity with 3 Pa hydrogen pressure and a sample holder bias voltage of −200 V.

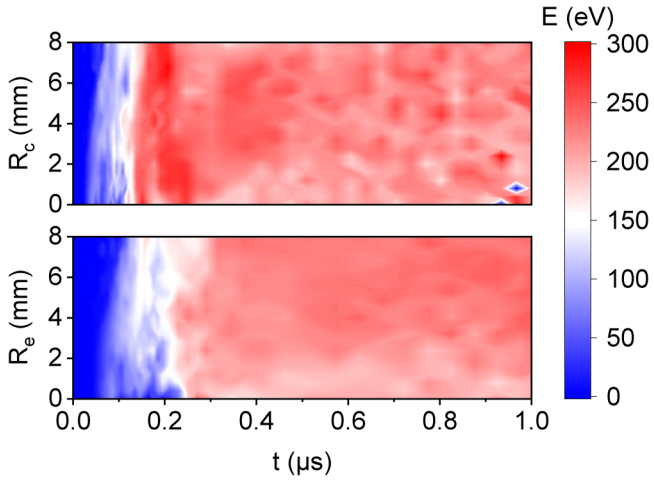

FIG. 8. H_3^+ attack energy along the sample radius for the cylindrical cavity (R_c) and ellipsoidal cavity (R_e).

ordinate is the distance from the center of the sample. From the onset of EUV irradiation, the energy of the H_3^+ attacking the sample surface increases rapidly. In the cylindrical cavity, the potential in the cavity rises rapidly after the irradiation (200 ns in Fig. 5), and the initial potential of the new ions is high. When these ions sputter the sample surface (from 100 to 300 ns), the statistical values of energy (~300 eV) are higher than expected. After the charge distribution stabilizes, the attack energy drops to the expected value of about 200 eV. The electric field variation in the ellipsoidal cavity is relatively gentle, and the ion attack energy at the sample surface rises steadily and remains around 200 eV, which is more controllable.

However, the improvement of the plasma yield has not become more effective in continuously reducing the aperture. In our model, a more stable electric field is obtained by further reducing the aperture diameter to 8 mm, but it is insufficient to augment the SE energy reach to the point where SEs can ionize hydrogen molecules.

Therefore, a reasonable cavity structure is key to improving the plasma yield and providing stable ion sputtering.

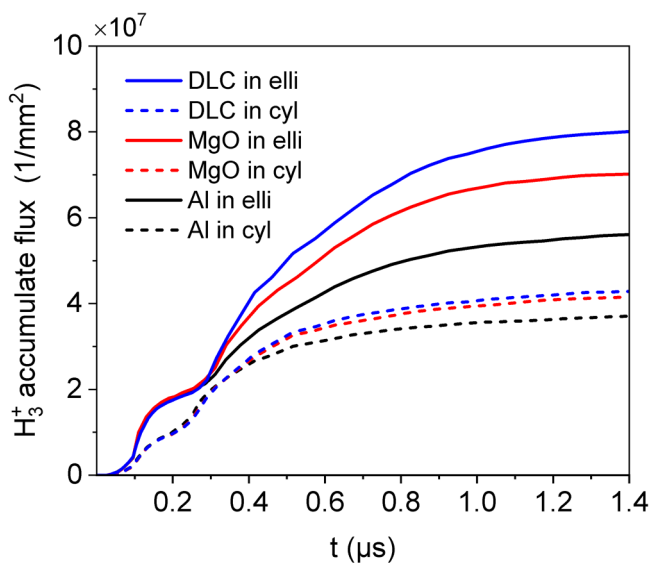

FIG. 9. Simulated the accumulated fluxes of H_3^+ at the sample for different cavity structures and different surface materials.

C. Influence of surface SEE characteristics

As mentioned in Sec. IV A, more SEs generated from the cavity surface can induce more plasma. Surface treatment is the most effective method to improve the SEE from the cavity surface. Figure 9 shows the accumulated fluxes of H_3^+ at the sample surface for different cavity structures and different surface treatments with a hydrogen pressure of 3 Pa and a sample holder bias voltage of −200 V. Comparing the case of different surface characteristics for the same cavity structure, no difference appears in the ion flux directly generated by photoionization (the first 200–300 ns), but the later flux increases due to SE ionization. The higher the SEY of the material, the more significant the increase in plasma density. Moreover, the elliptical cavity structure can better reflect the advantages of high-SEY materials.

The plasma can be obtained more efficiently by treating the surface of the cavity to improve the secondary electron yield in this scheme. Thus, appropriate cavity structure design and surface treatment to improve the SEE can significantly increase the upper limit of ion flux at the MLM surface for a given hydrogen pressure.

D. Influence of sample holder bias voltage

Changing the bias voltage of the sample holder controls the energy of the photoelectron impact at the cavity surface and the ion sputtering at the MLM surface and affects the potential distribution and thus the transport of charged particles in the cavity. The efficiency of ion sputtering, which can be controlled by varying the bias voltage applied to the sample holder, was also simulated.

According to Fig. 4, the most significant SEs will be induced from the surface of materials when the energy of incident electrons is close to E_m. Figure 10 shows the simulation results of ion fluxes on the sample surface under different bias voltages applied to the holder in an ellipsoidal cavity whose surface is treated with ALD MgO ($\delta_m \approx 4.9$, and $E_m \approx 550$ eV in Fig. 4). H_3^+ ions sputter mainly in the irradiated area of the sample surface (R < 2 mm), and the ion flux at the center is the largest.

The ion flux on the sample decreases significantly after the absolute value of the voltage exceeds 300 V. It indicates that the ion flux at the sample surface is related not only to the SEY but also to other factors. The average energy of photoelectron, E_{pe}, impacting the cavity depends on the negative bias U, e.g., E_{pe} is about −200 eV when U = −200 V. Obtain the maximum yield of SE from the cavity surface at U = −550 V. However, with the increase of the absolute value of negative bias, the electric field component

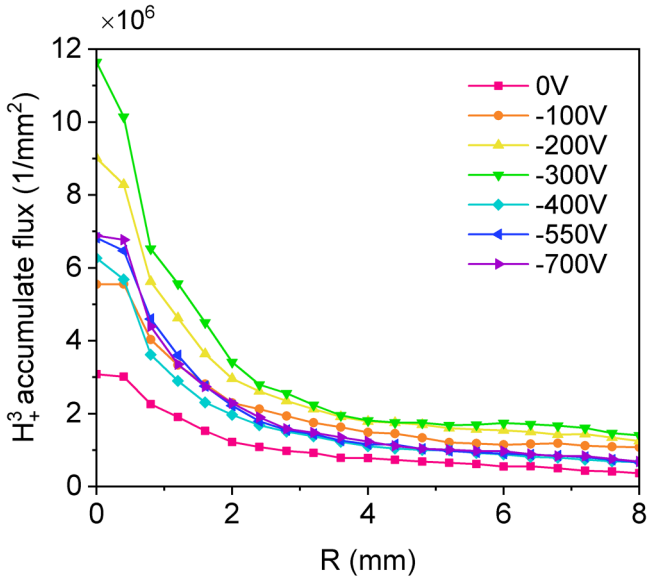

FIG. 10. Comparison of radial H_3^+ fluxes accumulated on the sample surface during an EUV pulse and for different sample holder bias voltages.

perpendicular to the sample surface also increases and applies more upward force to the SEs. Most SEs disappear across the aperture or are absorbed in the cavity surface before obtaining the energy required for ionizing hydrogen. Therefore, the increase in plasma density caused by SEs is limited. This analysis indicates the effects of applied bias on SEs, including the obtained energy and their flow.

A positive bias was also simulated, and the results indicate that the electric field, in this case, suppressed the ion sputter flux and energy, thereby preventing over-cleaning.

Table IV summarizes the total fluxes of H_3^+ per hour at the center of the sample surface under different conditions. As can be seen, the effects of cavity structure, surface SEY characteristics, and bias voltage on the flux of sputtering ions are more prominent. Compared with the surface-untreated cylindrical aluminum cavity, the ions sputtering flux on the sample in the surface-treated (improved SEY) ellipsoidal cavity is increased more than double under 3 Pa hydrogen pressure and −200 V holder bias. The optimized scheme can efficiently generate plasma and thus enhance EUV-induced plasma carbon cleaning at low pressure.

V. CONCLUSION

This work studies the evolution of EUV-induced plasma in the structure shown in Fig. 1 using the two-dimensional cylindrical symmetric coordinates PIC-MCC method. In our model, we carefully consider photoelectrons produced by EUV irradiating MLM and secondary electrons produced by electrons impacting solid and the role of these electrons in EUV-induced plasma. *In situ* and non-destructive cleaning of carbon contamination on the MLM surface by EUV-induced plasma in EUVL tools requires controlling ion sputtering flux and energy at the MLM surface.

The structure of the grounded cavity determines the distribution and variation of the electric field in the cavity. The generation of secondary electrons supplements the negative charge in the plasma and increases the density of the plasma. We investigated how SEs affect plasma evolution by optimizing the structure of the grounded cavity, treating the cavity surface, and changing the bias voltage applied to the sample holder.

The results indicate that, after the electrons gain energy in the electric field, the plasma density can be further increased via ionization collision, and then the ion sputtering on the surface of MLM can be enhanced. For this scheme, which controls the sputtering of plasma on the surface of MLM online by adjusting the bias voltage, we optimized the cavity structure into a reasonable ellipsoid and treated its inner surface to enhance the yield and the

TABLE IV. The total ion fluxes in the focus spot under different conditions. "DLC" refers to "diamond-like carbon."

Pressure (Pa)	Configuration of the grounded cavity	Surface properties	Bias voltage (V)	H_3^+ flux in focus spot (10^{13} mm^{-2} h)
1	Cylinder	Al	−200	0.57
3	Cylinder	Al	200	0.04
3	Cylinder	Al	100	0.28
3	Cylinder	Al	0	0.56
3	Cylinder	Al	−200	1.50
5	Cylinder	Al	−200	3.27
3	Ellipsoid	Al	−200	2.49
3	Ellipsoid	ALD MgO	0	1.00
3	Ellipsoid	ALD MgO	−100	2.00
3	Ellipsoid	ALD MgO	−200	3.25
3	Ellipsoid	ALD MgO	−300	4.19
3	Ellipsoid	ALD MgO	−400	2.71
3	Ellipsoid	B-doped DLC	−200	3.88
5	Ellipsoid	B-doped DLC	−200	7.75

emission persistence of the SE. A stable and efficient control scheme for EUV-induced plasma is obtained.

ACKNOWLEDGMENTS

The work was supported by the National Natural Science Foundation of China (Nos. 61974142 and 62104224), the "Xu-Guang" Talent Program of Changchun Institute of Optics, Fine Mechanics and Physics (CIOMP), Chinese Academy of Science (CAS) (No. E01672Y6Q0), and The Open Fund of State Key Laboratory of Applied Optics (No. SKLAO2020001A09).

AUTHOR DECLARATIONS

Conflict of Interest

The authors have no conflicts to disclose.

DATA AVAILABILITY

The data that support the findings of this study are available from the corresponding author upon reasonable request.

REFERENCES

[1]J. Hollenshead and L. Klebanoff, "Modeling radiation-induced carbon contamination of extreme ultraviolet optics," J. Vac. Sci. Technol. B **24**(1), 64–82 (2006).
[2]K. Boller, R.-P. Haelbich, H. Hogrefe, W. Jark, and C. Kunz, "Investigation of carbon contamination of mirror surfaces exposed to synchrotron radiation," Nucl. Instrum. Methods Phys. Res. **208**(1), 273–279 (1983).
[3]H. Meiling, V. Banine, P. Kuerz, B. D. Blum, G. J. Heerens, and N. Harned, "The EUV program at ASML: An update," Proc. SPIE **5037**, 24–35 (2003).
[4]B. V. Yakshinskiy, R. Wasielewski, E. Loginova, and T. E. Madey, "Carbon accumulation and mitigation processes, and secondary electron yields of ruthenium surfaces," Proc. SPIE **6517**, 65172Z (2007).
[5]V. Banine and J. Benschop, "EUV lithography: Main challenges," Proc. SPIE **5401**, 1–7 (2004).
[6]E. Louis, A. E. Yakshin, T. Tsarfati, and F. Bijkerk, "Nanometer interface and materials control for multilayer EUV-optical applications," Prog. Surf. Sci. **86**(11), 255–294 (2011).
[7]R. M. van der Horst, S. Nijdam, J. Beckers, and G. M. W. Kroesen, "Exploring the temporally resolved electron density evolution in EUV induced plasmas," J. Phys. D: Appl. Phys. **47**, 302001 (2014).
[8]R. M. van der Horst, J. Beckers, E. A. Osorio, and V. Y. Banine, "Dynamics of the spatial electron density distribution of EUV-induced plasmas," J. Phys. D: Appl. Phys. **48**(43), 432001 (2015).
[9]A. Dolgov, D. Lopaev, T. Rachimova, A. Kovalev, A. Vasil'Eva, C. J. Lee, V. M. Krivtsun, O. Yakushev, and F. Bijkerk, "Comparison of H_2 and He carbon cleaning mechanisms in extreme ultraviolet induced and surface wave discharge plasmas," J. Phys. D: Appl. Phys. **47**, 065205 (2014).
[10]A. Dolgov, O. Yakushev, A. Abrikosov, E. Snegirev, V. M. Krivtsun, C. J. Lee, and F. Bijkerk, "Extreme ultraviolet (EUV) source and ultra-high vacuum chamber for studying EUV-induced processes," Plasma Sources Sci. Technol. **24**, 035003 (2015).
[11]D. I. Astakhov, W. J. Goedheer, C. J. Lee, V. V. Ivanov, V. M. Krivtsun, K. N. Koshelev, D. V. Lopaev, R. M. Van Der Horst, J. Beckers, and E. A. Osorio, "Exploring the electron density in plasma induced by EUV radiation: II. Numerical studies in argon and hydrogen," J. Phys. D: Appl. Phys. **49**, 295204 (2016).
[12]A. Abrikosov, V. Reshetnyak, D. Astakhov, A. Dolgov, O. Yakushev, D. Lopaev, and V. Krivtsun, "Numerical simulations based on probe measurements in EUV-induced hydrogen plasma," Plasma Sources Sci. Technol. **26**, 045011 (2017).
[13]C. K. Birdsall and A. B. Langdon, *Plasma Physics* via *Computer Simulation* (Hilger, London, 1991).
[14]Y. Yamamura and H. Tawara, "Energy dependence of ion-induced sputtering yields from monatomic solids at normal incidence," At. Data Nucl. Data Tables **62**, 149–253 (1996).
[15]M. H. Van der Velden, W. J. M. Brok, J. J. A. M. Van der Mullen, W. J. Goedheer, and V. Banine, "Particle-in-cell Monte Carlo simulations of an extreme ultraviolet radiation driven plasma," Phys. Rev. E **73**, 036406 (2006).
[16]G. Dujardin, M. J. Besnard, L. Hellner, and Y. Malinovitch, "Double photoionization of H_2: An experimental test of electronic-correlation models in molecules," Phys. Rev. A **35**, 5012–5019 (1987).
[17]H. Kossmann, O. Schwarzkopf, B. Kammerling, W. Braun, and V. Schmidt, "Photoionisation cross section of H_2," J. Phys. B: At. Mol. Opt. Phys. **22**, L411–L414 (1989).
[18]Y. M. Chung, E.-M. Lee, T. Masuoka, and J. A. R. Samson, "Dissociative photoionization of H_2 from 18 to 124 eV," J. Chem. Phys. **99**, 885–889 (1993).
[19]T. W. Shyn and W. E. Sharp, "Angular distributions of electrons elastically scattered from H_2," Phys. Rev. A **24**, 1734–1740 (1981).
[20]J.-S. Yoon, M.-Y. Song, J.-M. Han, S. H. Hwang, W.-S. Chang, B. Lee, and Y. Itikawa, "Cross sections for electron collisions with hydrogen molecules," J. Phys. Chem. Ref. Data **37**, 913–931 (2008).
[21]T. Oka, "Interstellar," Chem. Rev. **113**, 8738–8761 (2013).
[22]S. Bajt, J. B. Alameda, T. W. Barbee, Jr., W. M. Clift, J. A. Folta, B. B. Kaufmann, and E. A. Spiller, "Improved reflectance and stability of Mo/Si multilayers," Opt. Eng. **41**(8), 1797–1804 (2002).
[23]T. E. Madey, N. S. Faradzhev, B. V. Yakshinskiy, and N. V. Edwards, "Surface phenomena related to mirror degradation in extreme ultraviolet (EUV) lithography," Appl. Surf. Sci. **253**, 1691–1708 (2006).
[24]B. L. Henke, J. A. Smith, and D. T. Attwood, "0.1-10keV x-ray-induced electron emissions from solids—Models and secondary electron measurements," J. Appl. Phys. **48**, 1852–1866 (1977).
[25]K. Kanaya, S. Ono, and F. Ishigaki, "Secondary electron emission from insulators," J. Phys. D: Appl. Phys. **11**, 2425–2437 (1978).
[26]S. Tao, H. Chan, and H. Van der Graaf, "Secondary electron emission materials for transmission dynodes in novel photomultipliers: A review," Materials **9**, 1017 (2016).
[27]A. Shih, J. Yater, C. Hor, and R. Abrams, "Secondary electron emission studies," Appl. Surf. Sci. **111**(1997), 251–258 (1997).
[28]Y. Lin and D. C. Joy, "A new examination of secondary electron yield data," Surf. Interfaces Anal. **37**, 895–900 (2005).
[29]H. P. Winter, F. Aumayr, and G. Lakits, "Recent advances in understanding particle-induced electron emission from metal surfaces," Nucl. Instrum. Methods Phys. Res. Sect. B **58**(3–4), 301–308 (1991).
[30]D. I. Astakhov, W. J. Goedheer, C. J. Lee, V. V. Ivanov, V. M. Krivtsun, A. I. Zotovich, S. M. Zyryanov, D. V. Lopaev, and F. Bijkerk, "Plasma probe characteristics in low density hydrogen pulsed plasmas," Plasma Sources Sci. Technol. **24**, 055018 (2015).
[31]R. M. van der Horst, "Electron dynamics in EUV-induced plasmas," Ph.D. thesis (Technische Universiteit Eindhoven, 2015).
[32]D. Astakhov, "Numerical study of extreme-ultra-violet generated plasmas in hydrogen," Ph.D. thesis (University of Twente, Twente, 2016).